UDK 669.721.5:546.11
Original scientific article/Izvirni znanstveni članek

ISSN 1580-2949
Mater. Tehnol.

FIRST-PRINCIPLE CALCULATIONS OF THE SYNERGISTIC CATALYTIC PERFORMANCE OF GRAPHENE AND TRANSITION METALS FOR MgH_2 DEHYDROGENATION

SINERGIČNA KATALITIČNA UČINKOVITOST GRAFENA IN PREHODNIH KOVIN POTREBNA ZA DEHIDROGENACIJO MgH_2, IZRAČUNANA PO PRVEM NAČELU

Xiaoming Du[1], Xiaolong Yin[1], Haicheng Liang[1*], Tianfu Li[2]

[1]School of Materials Science and Engineering, Shenyang Ligong University, Shenyang 110159, China
[2]China Institute of Atomic Energy, Beijing 102413, China

Prejem rokopisa – received: 2025-11-03; sprejem za objavo – accepted for publication: 2026-01-28

doi:10.17222/mit.2025.1604

To address the challenges of high dehydrogenation temperature and sluggish kinetics in magnesium hydride (MgH_2), this study systematically investigates the synergistic catalytic effects of transition metals (Ni, Fe, Cu, Cr, Sc) anchored on monolayer graphene in enhancing the dehydrogenation performance of magnesium-based hydrogen storage materials. First-principles calculations were performed using density functional theory (DFT) within the generalized gradient approximation (GGA), combined with a double numerical plus polarization (DNP) basis set. The computational results demonstrate that Ni-, Cr-, and Cu-modified graphene substrates significantly reduce both the dehydrogenation enthalpy and reaction energy barrier of Mg_4H_8 clusters. Charge density analysis, density of states, and differential charge density calculations were employed to elucidate the electronic interactions and charge redistribution within these systems. These analyses confirm a substantial weakening of the Mg–H bonds in Mg_4H_8, which effectively facilitates hydrogen desorption. Comprehensive evaluation based on thermodynamic and kinetic parameters, including dehydrogenation enthalpy, activation energy, and electronic structure features, establishes that the Cu/graphene composite doping exhibits the most pronounced improvement, achieving the optimal dehydrogenation performance of MgH_2. This work provides valuable theoretical insights and predictive guidance for the rational design of high-efficiency catalytic systems in magnesium-based hydrogen storage applications.

Keywords: hydrogen storage materials, MgH_2, graphene, first-principles calculations

Da bi se spopadli z izzivi visoko temperaturne dehidrogenacije in počasne kinetike v magnezijevem hidridu (MgH_2) so avtorji tega članka izvedli študijo, ki sistematično raziskuje sinergistične katalitične učinke prehodnih kovin (Ni, Fe, Cu, Cr, Sc), zasidranih na monoslojnem grafenu. Zato, da bi izboljšali dehidrogenacijske lastnosti materialov za shranjevanje vodika na osnovi magnezija so avtorji izvedli izračune po prvem načelu. Ti temeljijo na teoriji funkcionalne gostote (DFT) znotraj posplošenega gradientnega približka (GGA), v kombinaciji z baznim naborom dvojne numerične in polarizacijske metode (DNP). Računalniški rezultati so pokazali, da z Ni, Cr in Cu modificirani grafenski substrati znatno zmanjšajo tako entalpijo dehidrogenacije kot tudi reakcijsko energijsko pregrado grozdov Mg_4H_8. Za razjasnitev elektronskih interakcij in prerazporeditve naboja znotraj teh sistemov so avtorji uporabili analizo gostote naboja, gostote stanj in izračune diferencialne gostote naboja. S temi analizami so potrdili znatno oslabitev vezi Mg–H v Mg_4H_8, kar učinkovito olajša desorpcijo vodika. Celovita ocena, ki temelji na termodinamičnih in kinetičnih parametrih, vključno z entalpijo dehidrogenacije, aktivacijsko energijo in značilnostmi elektronske strukture so ugotovili, da dopiranje s kompozitom Cu/grafen pride do največjega izboljšanja, saj se dosega optimalna učinkovitost dehidrogenacije MgH_2. S to raziskavo so avtorji podali dragocene teoretične vpoglede in napovedne smernice za racionalno načrtovanje visoko učinkovitih katalitičnih sistemov za shranjevanje vodika na osnovi magnezija.

Ključne besede: materiali za shranjevanje vodika, MgH_2, grafen, izračuni na osnovi temeljnih principov

1 INTRODUCTION

In the context of intensifying global environmental challenges and the persistent depletion of conventional energy resources, human society is confronted with unprecedented energy demands. According to relevant data, proven global petroleum reserves are sufficient for only about half a century of consumption, while coal and natural gas resources are expected to be gradually exhausted within the next century. Since the last century, the large-scale use of the three primary fossil fuels – petroleum, coal, and natural gas – has caused atmospheric CO_2 concentrations to increase by nearly 50 % compared to pre-industrial levels, exceeding 420 ppm. This rise is primarily due to greenhouse gas emissions, particularly carbon dioxide, resulting from fossil fuel combustion. Consequently, extreme weather events have become increasingly frequent worldwide.[1–3] Hydrogen energy, recognized as an ideal energy source due to its high calorific value and zero pollution, has attracted significant attention in recent years. However, safe and efficient hydrogen storage technology is still the core bottleneck of its large-scale application.[4,5] However, the safe and efficient storage and transportation of hydrogen remain criti-

*Corresponding author's e-mail:
hcliang1976@sylu.edu.cn (H.C. Liang)

cal bottlenecks hindering its large-scale application. Solid-state hydrogen storage materials, especially magnesium-based hydrogen storage materials, are considered among the most promising candidates because of their high hydrogen storage capacity, abundant natural resources, and low cost.[6,7]

Among these, magnesium hydride (MgH_2) has garnered extensive interest owing to its high gravimetric (7.6 *w*/%) and volumetric (110 kg/m^3) hydrogen storage densities, enhanced safety profile, and the abundant availability of magnesium as a raw material. Compared to magnesium-based materials modified solely by nanostructuring or alloying (such as Mg_2NiH_4, whose pure phase still exhibits a high dehydrogenation temperature and requires high-concentration doping to achieve approximately 25% reduction in desorption temperature), as well as transition metal (TM)-only doped MgH_2 systems without carrier support (which are prone to issues such as TM particle agglomeration and diminished catalytic efficiency), the 'transition metal–graphene' composite-modified MgH_2 system in this study demonstrates superior synergistic effects. On the one hand, the high specific surface area and conductivity of graphene facilitate the dispersion of TM particles (e.g., Ni, Cr, Cu), thereby preventing agglomeration. On the other hand, the chemical interactions between the d-orbitals of TMs and H atoms, combined with graphene-mediated electron transfer, more significantly weaken the Mg–H bonds. Nevertheless, a practical application of MgH_2 is severely constrained by its excessively high thermodynamic stability and sluggish hydrogen absorption/desorption kinetics.[8–9]

To enhance the hydrogen storage properties of MgH_2, researchers have explored various strategies, including nanostructuring, alloying, and catalyst doping. Among these, the introduction of catalysts has been identified as one of the most effective approaches. In recent years, carbon materials, particularly graphene, have demonstrated significant potential in catalytic applications due to their unique two-dimensional structure, excellent electrical conductivity, and versatile surface chemistry.[10] Studies have indicated that graphene can serve as an efficient catalytic support, markedly improving the hydrogen absorption/desorption kinetics of MgH_2.[11–13] Moreover, transition metal (TM) doping has been demonstrated as one of the most effective strategies for precisely modulating the strength of Mg–H bonds. The vacant d-orbitals of TMs can engage in chemical interactions with H atoms, which not only weakens the covalent and ionic characteristics of Mg–H bonds, thereby reducing the dehydrogenation enthalpy, but also facilitates the dissociation and diffusion of H atoms, leading to a decrease in the reaction activation energy. Zhu et al.[14,15] studied Sc and Cu/Zn co-doping of Mg_2Ni-based hydrogen storage alloys. DFT calculations show that doping causes lattice expansion, inhibits hydrogen adsorption layers, and improves hydrogen kinetics. Cu/Zn atoms attract H and weaken H–Ni bonds, reducing stability and desorption temperature. Sc doping weakens H–Ni/Mg bonds and enhances hydrogen release. Optimal Sc concentration is $x = 0.25$.

Du et al.[16] employed first-principles calculations to investigate the effect of Y/Cu and Y/Zn co-doping on the dehydrogenation properties of Mg_2Ni hydrides. The results indicate that the $Mg_{1.25}Y_{0.75}Ni_{1-x}TM_x$ (TM = Cu/Zn) system undergoes lattice expansion with increasing TM content, which effectively weakens the critical Ni–H bonding interactions. This weakening contributes to a reduction in both the hydride stability and the dehydrogenation temperature. Remarkably, at a doping concentration of 50 %, the dehydrogenation temperature of the co-doped hydride is reduced by up to 25 % compared to pristine Mg_2NiH_4, demonstrating significantly enhanced catalytic dehydrogenation performance. Khatabi et al.[17] employed density functional theory (DFT) to investigate the mechanism by which doping with 3d and 4d transition metal elements – such as Sc, Ti, Cu, Cr, Y, Zr, Ni and Mo – enhances the hydrogen storage properties of MgH_2. Their study revealed that doping with these transition metal elements reduces the electron density between Mg and H atoms, leading to a weakening of the Mg–H bond energy. Furthermore, it was demonstrated that higher electronegativity or greater chemical reactivity of the doped transition metal elements results in a weaker Mg–H bond, thereby reducing the dehydrogenation enthalpy and activation energy of MgH_2. However, the underlying microscopic mechanism of graphene-catalyzed dehydrogenation in magnesium-based hydrogen storage materials remains incompletely understood and requires further in-depth investigation.

Xia et al.[18] successfully synthesized a composite material consisting of Ni-decorated graphene doped with MgH_2 nanoparticles. The MgH_2 particles were uniformly distributed across the surface and interlayers of graphene. This configuration effectively suppressed the agglomeration of MgH_2 during hydrogen storage cycles. Under the catalytic influence of Ni, the composite released 5.4 *w*/% of hydrogen within 30 min at 250 °C, demonstrating that graphene can act synergistically with other catalysts to modify magnesium-based hydrogen storage materials and enhance their dehydrogenation performance. Furthermore, the high thermal conductivity of graphene facilitates efficient heat transfer, thereby improving the rates of hydrogen adsorption and desorption, which contributes to superior hydrogen storage properties.

Owing to the presence of vacant d-orbitals capable of forming chemical bonds, transition metals facilitate charge transfer and bond formation, resulting in a strong affinity for hydrogen atoms. During the dissociation of hydrogen molecules or the recombination of hydrogen atoms, electron transfer occurs between the d-orbitals of transition metals and the molecular or atomic orbitals of

hydrogen. The resulting interactions significantly reduce the activation energy required for hydrogen dissociation or recombination, thereby enhancing the hydrogen absorption/desorption properties of magnesium-based materials.[19] Using first-principles calculations, Zhang et al.[20] investigated the catalytic effects of transition metals (TMs) and transition metal halides supported on graphene for improving the dehydrogenation performance of magnesium hydride (MgH_2). Their computational results confirmed that graphene modified with these species exhibits promising catalytic activity in enhancing the desorption properties of MgH_2. Specifically, Zhang et al.[20] reported the catalytic activity of graphene-supported Ni and $NiCl_2$ for MgH_2 dehydrogenation, achieving reduced desorption temperatures through structural regulation and charge transfer effects.

To further enhance the hydrogen absorption and desorption properties of MgH_2 and develop composite catalysts with synergistic effects, this study employs first-principles calculations based on density functional theory (DFT) to simulate and compute key parameters – including stable configurations, interaction energies, charge density differences, and dehydrogenation enthalpies – of MgH_2 cluster models supported on transition metal-decorated graphene. The influence of transition metal elements (Ni, Fe, Cu, Cr, and Sc) modified on graphene on the dehydrogenation performance of MgH_2 was systematically investigated, elucidating the underlying synergistic catalytic mechanism between graphene and transition metals in promoting hydrogen desorption from MgH_2. These findings provide new insights for the development of high-performance magnesium-based hydrogen storage materials.

2 COMPUTATIONAL DETAILS

First-principles calculations based on density functional theory (DFT) were performed using the Quantum ESPRESSO package.[21] This package employs the linear combination of atomic orbitals (LCAO) method combined with numerical basis sets to describe electron wave functions. Numerical basis sets offer high computational efficiency, making them particularly suitable for large molecular systems and periodic structures. The choice of basis sets significantly impacts computational accuracy and convergence.[22] In this study, the double numerical plus polarization (DNP) basis set was adopted to describe electron wave functions. The exchange-correlation energy was treated using the Perdew-Burke-Ernzerhof (PBE) functional within the generalized gradient approximation (GGA) framework.[23] The Kohn-Sham equations were solved iteratively through self-consistent field (SCF) calculations to obtain the electronic density and total energy of the system. The SCF iteration process continued until both electron density and energy converged to preset thresholds. The convergence criteria were set as follows: energy convergence threshold $E \leq 1.0\times10^{-5}$ Ha, stress convergence threshold $\alpha \leq 0.002$ Pa, and displacement convergence threshold $x \leq 0.0005$ nm. The cut-off energy and k-point grid were determined based on the inherent settings of the Quantum ESPRESSO package, which provides three quality tiers (low, medium, fine) for 2D system calculations instead of fixed numerical values. To ensure the highest precision of electronic structure and energy calculations, we selected the fine tier for both parameters: the cut-off energy is automatically optimized by the package's fine-tier configuration to achieve sufficient basis set expansion, and the k-point grid is preset as $3 \times 2 \times 1$ Monkhorst-Pack sampling (tailored for graphene-based 2D systems). Comparative verification was conducted: we tested low/medium-tier parameter combinations (e.g., $2 \times 1 \times 1$ k-point grid + medium cut-off energy) and confirmed that the fine-tier settings yield energy differences $<1\times10^{-5}$ Ha.

3 RESULTS AND DISCUSSION

3.1 Construction and optimization of cluster models

To investigate the catalytic effects of pristine graphene and transition metal (Ni, Fe, Cu, Cr, Sc)-modified graphene on the dehydrogenation performance of magnesium hydride (MgH_2), six computational models were constructed, as shown in **Figure 1**. Pristine graphene exhibits a hexagonal honeycomb structure, with its 1×1 unit cell (primitive cell) containing two inequivalent carbon atoms located at the lattice positions (0,0,0) and (1/3,2/3,0), respectively. When constructing the model, it is expanded into a 4×4 supercell, where the in-plane dimensions along the x and y directions are four times those of the original 1×1 unit cell, and the arrangement of hexagonal rings within the plane is correspondingly extended. Consequently, the total number of carbon atoms in the resulting 4×4 supercell is calculated as the number of atoms in the 1×1 unit cell $\times 4 \times 4$, i.e., $2 \times 4 \times 4 = 32$. This aligns with the established standard in the literature that a 4×4 graphene supercell contains 32 carbon atoms, thereby ensuring compatibility of the model dimensions with existing references.[24] **Figure 1a** depicts an Mg_4H_8 cluster composed of four MgH_2 molecules. To further substantiate the model's reliability, a $(2 \times 1 \times 1)$ supercell of MgH_2 was constructed and subjected to energy calculations. The computed energy of the supercell was –21894.8293 eV, while that of the Mg_4H_8 cluster was –21894.9348 eV. The close agreement between these energy values, from the perspective of energy conservation and its correlation with structural stability, further confirms the rationality and reliability of the Mg_4H_8 cluster model employed in this study. This provides critical support for the validity of subsequent computational results derived from this model.

Figures 1b–f illustrate the adsorption configurations of the Mg_4H_8 cluster on Ni, Fe, Cu, Cr, and Sc-decorated monolayer graphene, respectively. There are three possi-

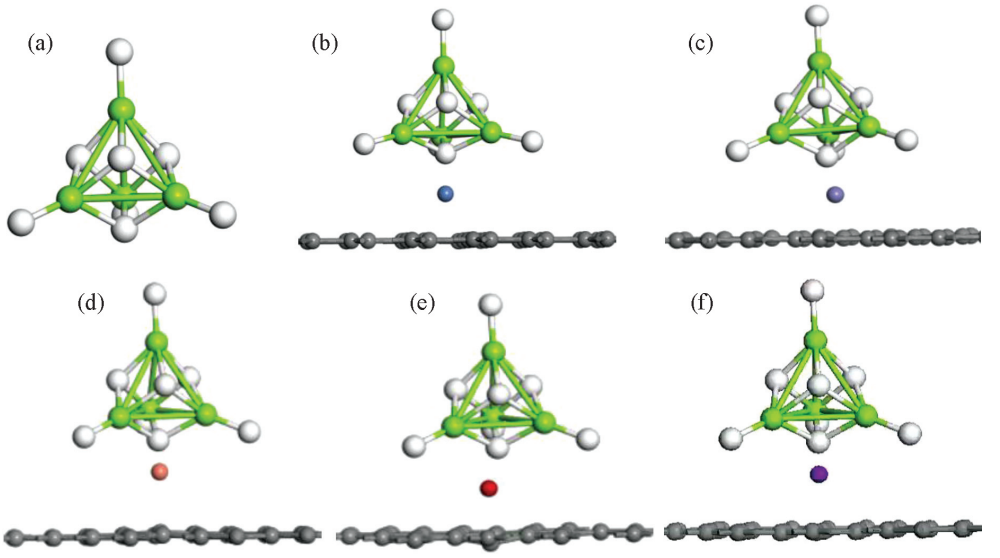

Figure 1: Computational models: a) Mg_4H_8 cluster, b) Mg_4H_8/Gr1-Ni, c) Mg_4H_8/Gr-Fe, d) Mg_4H_8/Gr1-Cu, e) Mg_4H_8/Gr1-Cr

ble adsorption sites for transition metal atoms on graphene substrates: top site, hollow site and bridge site. A vacuum layer of 2 nm was applied along the z-direction to avoid interactions between two neighboring slices. In this study, spin effects exert only a minor influence on the electronic structure of Ni. However, a comparative analysis of key interaction parameters – such as the degree of Mg–H bond weakening, dehydrogenation enthalpy changes, and reaction energy barriers – between the Gr–Ni system and Mg_4H_8 clusters, with and without spin polarization, reveals that these effects do not alter the overall catalytic trend of Gr–Ni in promoting MgH_2 dehydrogenation. Moreover, the relative order of catalytic performance among different transition metal-modified systems remains consistent. Therefore, to focus on elucidating the core mechanism of graphene–transition metal synergistic catalysis and to reduce computational complexity, spin polarization was not explicitly considered in the present work.

To identify the optimal adsorption sites of transition metal atoms (Ni, Cu, Fe, Cr, and Sc) on monolayer graphene, their adsorption energies (E_{ads}) at the most stable positions were calculated using Equations (1)–(5), respectively. Furthermore, the adsorption energies of Mg_4H_8 clusters on these five transition metal-modified graphene surfaces were evaluated with Equation (6) to confirm their structural stability.[25]

$$E_{ads}(Gr_{surface}+N_{atom} = \\ = E_{tot}(Gr_{surface}+N_{atom}) - E_{tot}(Gr_{surface}) - E_{tot}(Ni_{atom}) \quad (1)$$

$$E_{ads}(Gr_{surface}+Cu_{atom} = \\ = E_{tot}(Gr_{surface}+Cu_{iatom}) - E_{tot}(Gr_{surface}) - E_{tot}(Cu_{atom}) \quad (2)$$

$$E_{ads}(Gr_{surface}+Fe_{atom} = \\ = E_{tot}(Gr_{surface}+Fe_{atom}) - E_{tot}(Gr_{surface}) - E_{tot}(Fe_{atom}) \quad (3)$$

$$E_{ads}(Gr_{surface}+Cr_{atom} = \\ = E_{tot}(Gr_{surface}+Cr_{atom}) - E_{tot}(Gr_{surface}) - E_{tot}(Cr_{atom}) \quad (4)$$

$$E_{ads}(Gr_{surface}+Sc_{atom} = \\ = E_{tot}(Gr_{surface}+Sc_{atom}) - E_{tot}(Gr_{surface}) - E_{tot}(Sc_{atom}) \quad (5)$$

$$E_{ads}(Mg_4H_8/Gr) = \\ = E_{tot}(Mg_4H_8/Gr) - E_{tot}(Gr_{surface}) - E_{tot}(Mg_4H_8) \quad (6)$$

Here, $E_{tot}(Gr_{surface}+Ni_{atom})$, $E_{tot}(Gr_{surface}+Cu_{atom})$, $E_{tot}(Gr_{surface}+Fe_{atom})$, $E_{tot}(Gr_{surface}+Cr_{atom})$ and $E_{tot}(Gr_{surface}+Sc_{atom})$ are the total energies of monolayer graphene modified by Ni, Cu, Fe, Cr, and Sc atoms, respectively. $E_{tot}(Gr_{surface})$ is the total energy of the pristine monolayer graphene. To simplify the calculations, the total energies of all isolated atoms – Ni, Cu, Fe, Cr, and Sc, denoted as $E_{tot}(Ni_{atom})$, $E_{tot}(Cu_{atom})$,$E_{tot}(Fe_{atom})$, $E_{tot}(Cr_{atom})$ and $E_{tot}(Sc_{atom})$, respectively – were computed within a cubic vacuum supercell measuring (2 × 2 × 2) nm. $E_{tot}(Mg_4H_8/Gr)$ is the total energy of the system with an Mg_4H_8 cluster adsorbed on pristine or transition metal-modified graphene, $E_{tot}(Mg_4H_8)$ is the total energy of an isolated Mg_4H_8 cluster, and $E_{tot}(Gr)$ is the total energy of the pristine or transition metal-modified graphene substrate. The obtained total energies were substituted into Equations (1)–(6) to calculate the adsorption energies of monolayer graphene modified by Ni, Cu, Fe, Cr, and Sc at the top, bridge, and hollow sites. The calculated results for the adsorption energies of transition metals on graphene are plotted in **Figure 2**. It was found that the lowest adsorption energy of transition metal atoms Ni, Cu, Fe, Cr, and Sc on single-layer graphene is the hollow site. Only Cu is at the top. It can be concluded that the optimal adsorption sites for Ni, Fe, Cr, and Sc on graphene are the hollow sites, whereas the top site is most favorable for Cu. As also shown in **Figure 2**, Sc exhibits the lowest adsorption energy at all three sites, indicating that Sc adsorption on the graphene surface is the most stable. The lowest adsorption energy of Ni at the hollow site of graphene is –1.817 eV, which is close to the value of –1.9765 eV reported by Zhang et

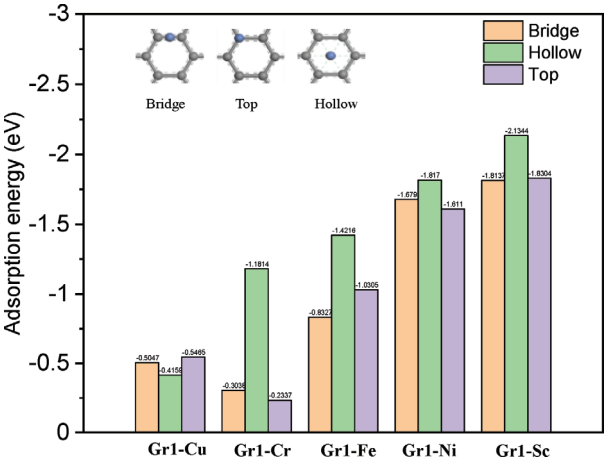

Figure 2: Adsorption energies of transition metals at different sites on monolayer graphene

al.,[20] thus validating the reliability of our computational framework.

The adsorption energies of the Mg_4H_8 cluster on Ni-, Fe-, Cu-, Cr-, and Sc-modified graphene surfaces were calculated to be –1.6062 eV, –1.6750 eV, –0.8739 eV, –2.5615 eV, and –2.1373 eV, respectively. A more negative adsorption energy indicates stronger system binding, superior structural stability, and greater suppression of cluster migration and agglomeration, thereby preserving the integrity of the catalytic interface. Among these systems, Mg_4H_8/Gr1–Cr exhibits the most negative adsorption energy (–2.5615 eV) and the highest structural stability, followed by Mg_4H_8/Gr1–Sc (–2.1373 eV). The Mg_4H_8/Gr1–Fe (–1.6750 eV) and Mg_4H_8/Gr1–Ni (–1.6062 eV) systems show moderate stability, yet both satisfy the structural requirements for dehydrogenation reactions. Although Mg_4H_8/Gr1–Cu has the least negative adsorption energy (–0.8739 eV) and the lowest structural stability, the adsorption process remains spontaneous. Furthermore, subsequent calculations confirm that this system exhibits the optimal catalytic performance without structural instability risks. In summary, all five composite systems possess satisfactory structural stability, providing a reliable model foundation for subsequent studies on dehydrogenation performance.

3.2 Dehydrogenation enthalpy and activation energy

As is well known, the dehydrogenation performance of hydrogen storage materials is closely related to the kinetic and thermodynamic properties of the system. According to the Van't Hoff equation[26] and the Arrhenius equation,[27] a decrease in dehydrogenation enthalpy or activation energy can lead to a reduction in dehydrogenation temperature and an increase in dehydrogenation rate. Therefore, to elucidate the underlying mechanism by which graphene and transition metal-modified graphene significantly enhance the dehydrogenation performance of MgH_2, it is essential to calculate and compare the dehydrogenation enthalpy and activation energy across different systems. The dehydrogenation enthalpies for the six models were evaluated using the following Equations, (7)–(12):[20]

$$\Delta H(Mg_4H_8) = E_{tot}(Mg_4) + 4E_{tot}(H_2) - E_{tot}(Mg_4H_8) \quad (7)$$

$$\Delta H(Mg_4H_8{+}Gr1{+}Ni) = E_{tot}(Mg_4{+}Gr1{+}Ni) + 4E_{tot}(H_2) - - E_{tot}(Mg_4H_8{+}Gr1{+}Ni) \quad (8)$$

$$\Delta H(Mg_4H_8{+}Gr1{+}Fe) = E_{tot}(Mg_4{+}Gr1{+}Fe) + 4E_{tot}(H_2) - - E_{tot}(Mg_4H_8{+}Gr1{+}Fe) \quad (9)$$

$$\Delta H(Mg_4H_8{+}Gr1{+}Cu) = E_{tot}(Mg_4{+}Gr1{+}Cu) + 4E_{tot}(H_2) - - E_{tot}(Mg_4H_8{+}Gr1{+}Cu) \quad (10)$$

$$\Delta H(Mg_4H_8{+}Gr1{+}Cr) = E_{tot}(Mg_4{+}Gr1{+}Cr) + 4E_{tot}(H_2) - - E_{tot}(Mg_4H_8{+}Gr1{+}Cr) \quad (11)$$

$$\Delta H(Mg_4H_8{+}Gr1{+}Sc) = E_{tot}(Mg_4{+}Gr1{+}Sc) + 4E_{tot}(H_2) - - E_{tot}(Mg_4H_8{+}Gr1{+}Sc) \quad (12)$$

where $E_{tot}(Mg_4H_8)$, $E_{tot}(Mg_4H_8{+}Gr1{+}Ni)$, $E_{tot}(Mg_4H_8{+}Gr1{+}Fe)$, $E_{tot}(Mg_4H_8{+}Gr1{+}Cu)$, $E_{tot}(Mg_4H_8{+}G{+}Cr)$, and E_{tot} $(Mg_4H_8{+}Gr1{+}Sc)$ are the total energies of the Mg_4H_8 cluster and the Mg_4H_8 cluster adsorbed on monolayer graphene surfaces modified with Ni, Cu, Fe, Cr, and Sc atoms, respectively. E_{tot} (Mg_4), E_{tot} $(Mg_4{+}Gr1{+}Ni)$, E_{tot} $(Mg_4{+}Gr1{+}Fe)$, E_{tot} $(Mg_4{+}Gr1{+}Cu)$, E_{tot} $(Mg_4{+}Gr1{+}Cr)$ and E_{tot} $(Mg_4{+}Gr1{+}Sc)$ are the total energies of the respective models after complete desorption of all hydrogen atoms. E_{tot} (H_2) is the total energy of an isolated hydrogen molecule.

The dehydrogenation enthalpies of the Mg_4H_8 cluster and its composite systems with Ni-, Fe-, Cu-, Cr-, and Sc-modified graphene were systematically calculated in this study, with the results presented in **Figure 3**. The dehydrogenation enthalpy of the pristine Mg_4H_8 cluster is 2.5761 eV. Upon forming the composite with Sc-modified graphene, the dehydrogenation enthalpy increases slightly, indicating that Sc inhibits the dehydrogenation process. In contrast, the composite with Fe-modified graphene exhibits a dehydrogenation enthalpy of 2.5434 eV, marginally lower than that of the pure Mg_4H_8 cluster. However, compared to the value of 2.5338 eV obtained in this study for the Mg_4H_8/single-layer graphene composite system, the introduction of Fe does not further reduce the dehydrogenation enthalpy. This suggests that Fe incorporation does not improve dehydrogenation kinetics. Conversely, the composites of Mg_4H_8 with Ni-, Cr-, and Cu-modified graphene exhibit significant reductions in dehydrogenation enthalpy, with values of 1.8659 eV, 1.7606 eV, and 1.2326 eV, respectively, corresponding to decreases of 27.6–52.1 %. This indicates that graphene modified with Ni, Cr, or Cu catalyzes the dehydrogenation performance of Mg_4H_8 more effectively. The enhancement observed with Ni-modified graphene aligns with the results reported by Huan Qingqing et al.[28] Quantitative analysis based on the Van't Hoff equation ($\ln P_{eq} = \Delta H/(RT) - \Delta S/R$) reveals that the reduction in dehydrogenation enthalpy directly lowers the equilibrium dehydrogenation temperature by approx-

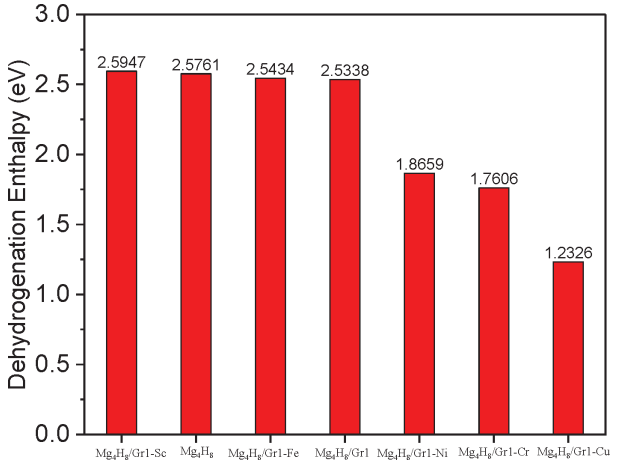

Figure 3: Hydrogen desorption enthalpy values for the six constructed models

imately 20–40 °C. As demonstrated by Huan Qingqing et al., the magnesium–nickel/graphene composite can fully desorb hydrogen within 1800 s at 280 °C, achieving a hydrogen desorption capacity of 6.05 %.

To further elucidate the influence of Ni, Cr, and Cu decoration on the dehydrogenation properties of magnesium hydride, dehydrogenation processes of the six model systems – Mg_4H_8, Mg_4H_8/Gr1-Sc, Mg_4H_8/Gr1-Fe, Mg_4H_8/Gr1-Ni, Mg_4H_8/Gr1-Cr, and Mg_4H_8/Gr1-Cu – were investigated in this work. In the Mg_4H_8 cluster, two types of hydrogen atoms exist: one bonded to a single Mg atom and another coordinated to three Mg atoms, denoted as H_1 and H_3, respectively. Previous studies indicate that in both pure Mg_4H_8 and graphene-doped Mg_4H_8 systems, desorption of the $H_1 + H_3$ pair exhibits a lower dehydrogenation enthalpy compared to other combinations.[29] To further clarify the kinetic advantages of transition metal-modified graphene in promoting Mg_4H_8 dehydrogenation, the nudged elastic band (NEB) method[30] was employed to calculate the reaction energy barriers and energy changes during the desorption of one H_2 molecule (targeting the $H_1 + H_3$ pair with relatively low dehydrogenation enthalpy) for each model system. The calculated results are presented in **Figure 4**. The pristine Mg_4H_8 cluster exhibits an extremely high reaction energy barrier of 4.4753 eV for H_2 desorption, which is consistent with its sluggish dehydrogenation kinetics reported in previous studies.[31] Among these systems, the activation energy results of each transition metal-modified system are as follows: Sc-modified system (2.1979 eV), Cu-modified system (2.6199 eV), Fe-modified system (2.8817 eV), Ni-modified system (3.1194 eV), and Cr-modified system (3.1312 eV). All data were acquired under unified calculation parameters and model optimization procedures to ensure consistency with the dehydrogenation enthalpy analysis.

From the aspect of kinetic performance, the activation energy of all transition metal-modified systems was lower than that of the pure Mg_4H_8 cluster (4.4753 eV), with the reduction range varying from 29.9 % (for the Cr-modified system) to 53.1 % (for the Sc-modified system). This confirms that the synergistic effect between transition metals and graphene can effectively reduce the reaction energy barrier and enhance dehydrogenation kinetics. Specifically, the Sc-modified system exhibited the lowest activation energy, corresponding to the theoretically fastest dehydrogenation rate; the Cu-modified system ranked second, demonstrating significant kinetic advantages; the activation energy of the Fe-, Ni-, and Cr-modified systems increased in sequence, and their kinetic promotion effects weakened gradually. However, combined with the previous dehydrogenation enthalpy data, it is clear that a single kinetic advantage cannot fully represent the overall performance: the dehydrogenation enthalpy of the Sc-modified system was slightly higher than that of the pure Mg_4H_8 cluster, which accelerated the reaction rate but increased thermodynamic en-

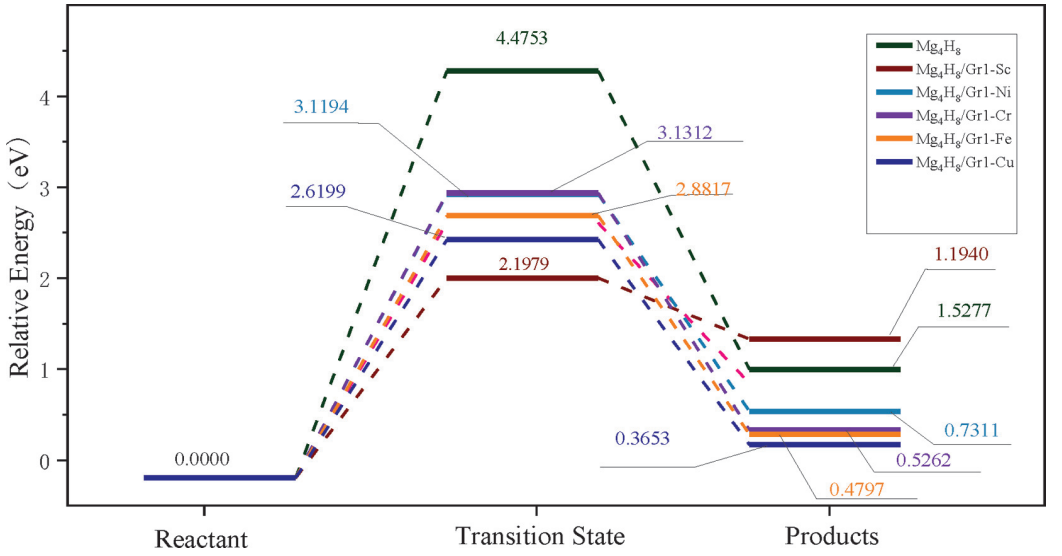

Figure 4: Energy changes for six dehydrogenation models

ergy consumption; the dehydrogenation enthalpy of the Fe-modified system (2.5434 eV) was only marginally lower than that of the pure cluster (2.5761 eV), leading to limited thermodynamic optimization. Consequently, neither of these two systems can meet the practical requirements of low energy consumption and fast reaction.

Based on the synergistic analysis of activation energy and dehydrogenation enthalpy, the Cu-, Ni-, and Cr-modified systems showed superior performance. The Cu-modified system not only maintained a relatively low activation energy (2.6199 eV) but also had its dehydrogenation enthalpy (1.2326 eV) reduced by 52.1 % compared with the pure cluster. Calculations based on the Van't Hoff equation indicated that the equilibrium dehydrogenation temperature could be decreased by approximately 40°C, realizing the dual optimization of low energy barrier and low enthalpy change. Although the activation energy of the Ni-modified system (dehydrogenation enthalpy: 1.8659 eV; activation energy: 3.1194 eV) and the Cr-modified system (dehydrogenation enthalpy: 1.7606 eV; activation energy: 3.1312 eV) was higher than that of the Sc- and Cu-modified systems, their dehydrogenation enthalpy was significantly reduced, and the activation energy was still approximately 30% lower than that of the pure cluster. Therefore, their performance balance was superior to that of the Sc- and Fe-modified systems.

In conclusion, based on the comprehensive evaluation of activation energy and dehydrogenation enthalpy, the Cu-modified graphene system, which exhibits both low activation energy and low dehydrogenation enthalpy, is identified as the optimal choice for regulating the dehydrogenation performance of Mg_4H_8 in this study. The Ni- and Cr-modified systems can be used as alternative schemes, while the Sc- and Fe-modified systems, due to the existence of kinetic-thermodynamic imbalance, are not the focus of the subsequent analysis.

3.3 Electronic structure

3.3.1 Electron density

To gain deeper insights into the catalytic mechanisms of Ni-, Cr-, and Cu-modified graphene in the dehydrogenation of Mg_4H_8, charge density analysis was performed on three adsorption models: Mg_4H_8/Gr1-Ni, Mg_4H_8/Gr1-Cr, and Mg_4H_8/Gr1-Cu, along with the isolated Mg_4H_8 cluster model. The fully relaxed configurations, including charge density distributions, are presented in **Figure 5**. As shown in **Figure 5a**, a noticeable electron density overlap exists between Mg and H atoms, suggesting the coexistence of ionic and covalent bonding within the cluster. When the Mg_4H_8 cluster is adsorbed onto transition metal (Ni, Cr, Cu)-modified monolayer graphene, distinct charge interaction regions form between the cluster, the transition metal atoms, and the graphene substrate, indicating chemical adsorption. In all three models, a significant charge density overlap is observed around the transition metal sites, demonstrating that the incorporation of Ni, Cr, and Cu promotes the charge transfer between the Mg_4H_8 cluster and the graphene support. Notably, as shown in **Figures 5c** and **5d**, the Mg_4H_8 cluster exhibits severe distortion after the adsorption on Cr- or Cu-modified graphene. This structural deformation of the cluster may affect the hydrogen release performance of the system. In contrast, no obvious distortion is observed for the Mg_4H_8 cluster adsorbed on Ni-modified graphene, as shown in **Figure 5b**.

3.3.2 Differential charge density

To investigate the charge transfer between the Mg_4H_8 cluster and graphene surfaces modified with different transition metal atoms, the charge density difference of the stabilized configurations was calculated using Equations (12)–(14):[32]

$$\Delta\rho_{Gr1-Ni} = \rho_{Mg_4H_8/Gr1-Ni} - (\rho_{Gr1-Ni} + \rho_{Mg_4H_8}) \quad (12)$$

$$\Delta\rho_{Gr1-Cr} = \rho_{Mg_4H_8/Gr1-Cr} - (\rho_{Gr1-Cr} + \rho_{Mg_4H_8}) \quad (13)$$

$$\Delta\rho_{Gr1-Cu} = \rho_{Mg_4H_8/Gr1-Cu} - (\rho_{Gr1-Cu} + \rho_{Mg_4H_8}) \quad (14)$$

where $\Delta\rho_{Gr1\text{-}Ni}$, $\Delta\rho_{Gr1\text{-}Cr}$ and $\Delta\rho_{Gr1\text{-}Cu}$ are the charge density differences between Ni-, Cr-, and Cu-modified graphene and Mg_4H_8 cluster, respectively, in C/m³; $\rho_{Mg4H8/Gr1\text{-}Ni}$, $\rho_{Mg4H8/Gr1\text{-}Cr}$, $\rho_{Mg4H8/Gr1\text{-}Cu}$ are the charge densities of the Mg_4H_8/Gr1-Ni, Mg_4H_8/Gr1-Cr, Mg_4H_8/Gr1-Cu systems, respectively, in C/m^3; $\rho_{Gr1\text{-}Ni}$, $\rho_{Gr1\text{-}Cr}$, $\rho_{Gr1\text{-}Cu}$ are the charge densities of the unperturbed Ni-, Cr-, and Cu-modified graphene surfaces, respectively, in C/m^3; and ρ_{Mg4H8} represents the charge density of the unperturbed Mg_4H_8 cluster, in C/m³. The differential charge densities of the fully relaxed Mg_4H_8/Gr1-Ni, Mg_4H_8/Gr1-Cr, and Mg_4H_8/Gr1-Cu models are shown in **Figure 6**. Blue regions indicate electron gain, while yellow regions indicate electron loss. As shown in **Figures 6a**, **6b** and **6c**, the areas surrounding the Ni, Cr, and Cu transition metal atoms exhibit significant electron loss. In contrast, electron accumulation is predominantly observed at the interfaces

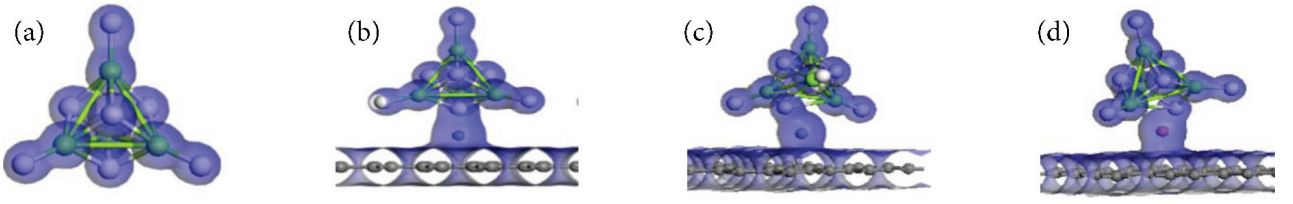

Figure 5: Charge density of four fully relaxed models: a) Mg_4H_8 cluster, b) Mg_4H_8/Gr_1-Ni, c) Mg_4H_8/Gr_1-Cr, d) Mg_4H_8/Gr_1-Cu

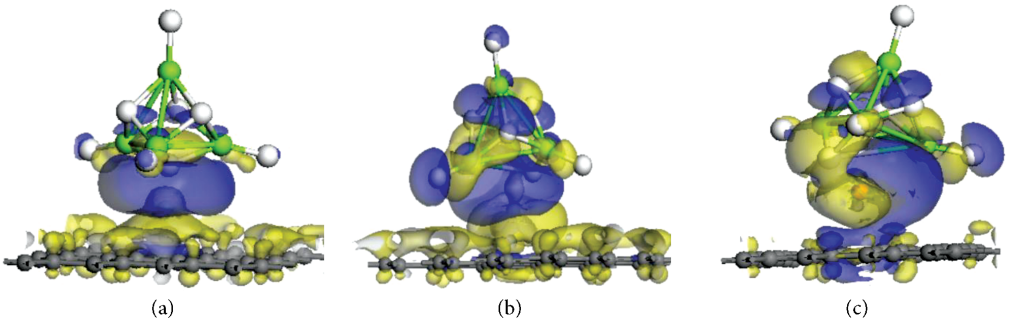

Figure 6: Differential charge density of the Mg_4H_8 cluster on three different transition metal-modified graphene substrates: a) Mg_4H_8/Gr1-Ni, b) Mg_4H_8/Gr1-Cr, c) Mg_4H_8/Gr1-Cu

Table 1: Bond lengths of the three Mg–H bonds adjacent to graphene and bonded to a single Mg atom in the five model systems

	Mg-H1(nm)	Mg-H2(nm)	Mg-H3(nm)	Average bond length
Mg_4H_8	0.1700	0.1702	0.1703	0.17016
Mg_4H_8/Gr1-Ni	0.1710	0.1711	0.1711	0.17107
Mg_4H_8/Gr1-Cr	0.1712	0.1718	0.1720	0.17167
Mg_4H_8/Gr1-Cu	0.1715	0.1718	0.1717	0.17167

between transition metal atoms and graphene, as well as between transition metal atoms and the Mg_4H_8 cluster – these localized electron-rich regions arise from the chemical adsorption and charge transfer interactions among the three components.

In **Figure 6a**, a small number of Mg and H atoms show electron gain, whereas the region between three Mg atoms and H atoms near the graphene exhibits electron loss, which is expected to affect the strength of the Mg–H bonds. In **Figures 6b** and **6c**, most Mg and H atoms nearby display electron gain, and the electron loss between Mg and H is more pronounced than in **Figure 6a**, with the most evident case being the Mg_4H_8/Gr1-Cu system (**Figure 6c**). The differential charge density results indicate that modifying graphene with transition metals (Ni, Cr, Cu) can weaken the Mg–H bond strength in the MgH_2 cluster. To further verify this conclusion, the H atoms bonded to the three Mg atoms closest to the graphene substrate in the Mg_4H_8 cluster are labeled H1, H2, and H3, as shown in **Figure 7**. The bond lengths of Mg–H1, Mg–H2, and Mg–H3 in the three models are listed in **Table 1**. The Mg–H bond lengths in the Mg_4H_8 cluster adsorbed on transition metal-modified graphene are all longer than those in the pure Mg_4H_8 cluster, with the bond length in Mg_4H_8 being consistent with the results reported in the relevant literature.[33] From **Table 1**, a clear trend in bond lengths is observed across the systems, in the order of Mg_4H_8/Gr1-Cu > Mg_4H_8/Gr1-Cr > Mg_4H_8/Gr1-Ni, further confirming that the Mg–H bond strength is weakened.

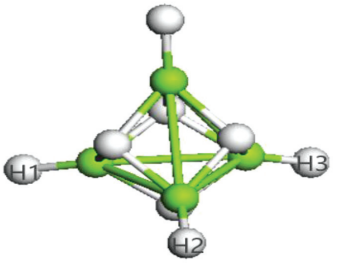

Figure 7: Position diagram of the three H atoms in the Mg–H bonds

3.3.3 State density analysis

To further investigate the catalytic mechanism of graphene and transition metal-modified graphene on the dehydrogenation performance of the Mg_4H_8 cluster, the total density of states (TDOS) and partial density of states (PDOS) of the Mg_4H_8 cluster, Mg_4H_8/Gr1, Mg_4H_8/Gr1-Ni, Mg_4H_8/Gr1-Cr, and Mg_4H_8/Gr1-Cu were analyzed, as shown in **Figure 8**. In **Figure 8a**, within the energy range from –6 eV to 9 eV, prominent hybridization peaks appear between the H-1s orbital and the Mg-3s and Mg-2p orbitals, indicating that the Mg–H bond is predominantly a strong covalent–ionic mixed bond. The high hybridization intensity implies strong bonding between H and Mg, requiring higher energy to release hydrogen (i.e., a higher dehydrogenation enthalpy). **Figure 8a** also shows that Mg_4H_8 has a band gap of 3.5 eV between the conduction and valence bands, indicating its pronounced non-metallic character. The density of states for Mg_4H_8/Gr1, Mg_4H_8/Gr1-Ni, Mg_4H_8/Gr1-Cr, and Mg_4H_8/Gr1-Cu are presented in **Figures 8b**, **8c**, **8d**, and **8e**, respectively. Compared with **Figure 8a**, the intensity of the hybridization peaks between Mg and H atoms is significantly reduced, indicating a weakened interaction between Mg and H.

The reduction in hybridization strength directly weakens the covalent character of the Mg–H bonds, making hydrogen more prone to desorption. However, in **Figures 8c**, **8d**, and **8e**, after modification with transition metals Ni, Cr, and Cu, the intensity of the bonding peaks in the TDOS of Mg_4H_8 is lower than that in **Figure 8b** for monolayer graphene-catalyzed Mg_4H_8, with the ex-

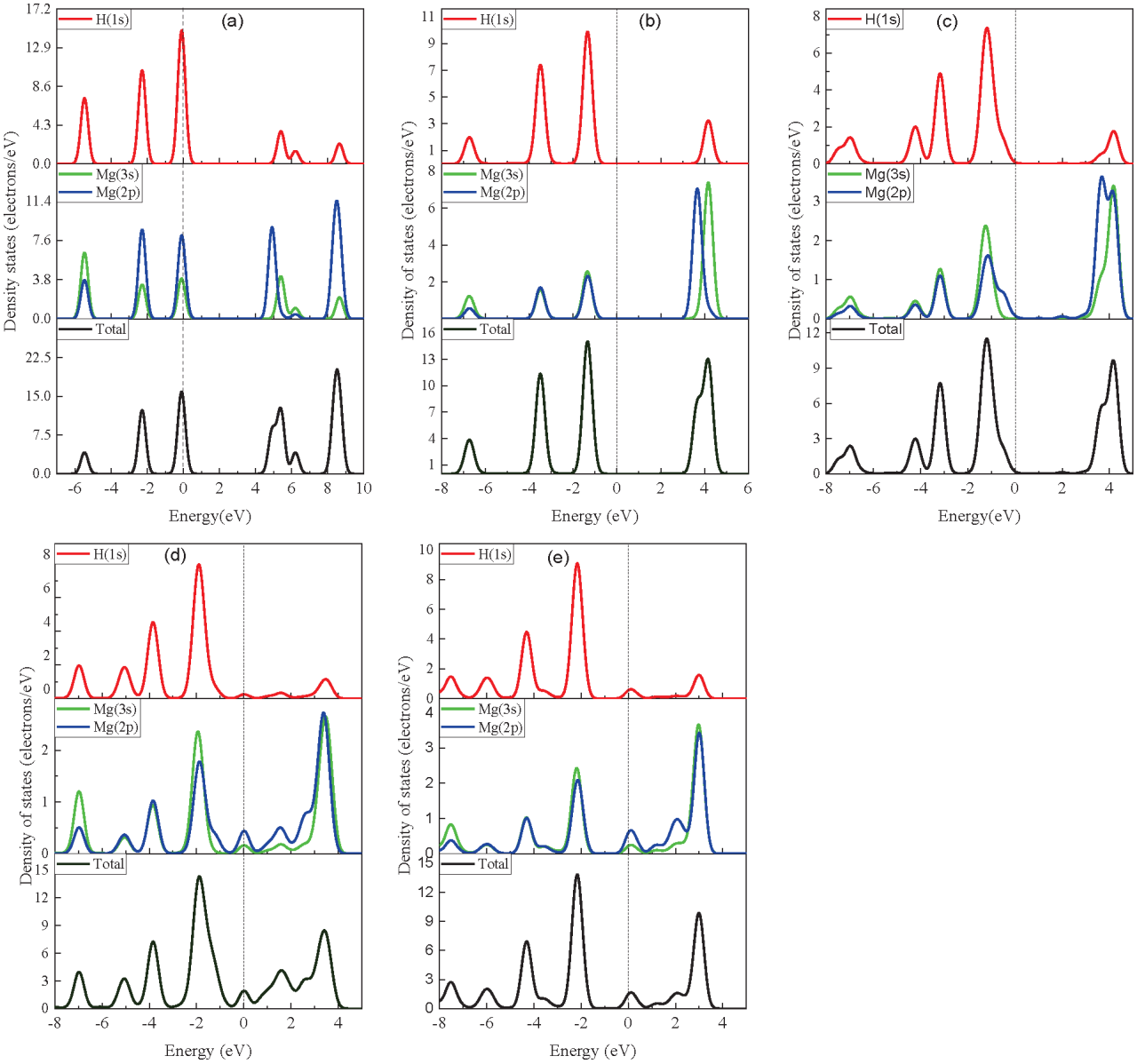

Figure 8: Total density of states (TDOS) and partial density of states (PDOS) for: a) Mg_4H_8 cluster, b) Mg_4H_8/Gr_1, c) Mg_4H_8/Gr_1-Ni, d) Mg_4H_8/Gr_1-Cr, e) Mg_4H_8/Gr_1-Cu

tent of bonding peak reduction following the order Cu > Cr > Ni. Moreover, after the catalysis by Ni-, Cr-, and Cu-modified monolayer graphene, the bonding peaks shift toward lower energy levels, and the PDOS of Mg and H also shift downward, indicating that the introduction of transition metals forms strong interactions with hydrogen, resulting in the formation of TM–H bonds. This weakens the original Mg–H bonds and facilitates hydrogen dissociation from the Mg atoms.

Based on the characteristics of the total density of states (TDOS) and partial density of states (PDOS) in **Figure 8**, the differences in electrical conductivity of different systems can be clarified from the perspectives of band gap and electronic state distribution at the Fermi level. For the pristine Mg_4H_8 cluster (**Figure 8 (a)**), the TDOS shows that the electronic state density at the Fermi level is 0, and the band gap between the highest occupied molecular orbital (HOMO) and the lowest unoccupied molecular orbital (LUMO) is approximately 3.5 eV, conforming to the typical characteristics of insulators – large band gap and no electronic states at the Fermi level. For the Mg_4H_8/Gr1 system (**Figure 8b**), due to the weak interaction between graphene and Mg_4H_8, the band gap is slightly narrower than that of the pristine Mg_4H_8. However, the electronic state density at the Fermi level remains low, and the system as a whole exhibits semiconductor-like properties. Regarding the transition metal-modified systems: In Mg_4H_8/Gr1-Ni (**Figure 8b**), the electronic interaction between Ni, Mg_4H_8, and graphene is weak, only partially filling the band gap of

Mg_4H_8. Only a small number of electronic states appear at the Fermi level, leading to weak metallicity rather than insulating properties. In contrast, in Mg_4H_8/Gr1-Cr (**Figure 8d**) and Mg_4H_8/Gr1-Cu (**Figure 8e**), the d-orbitals of Cr and Cu exhibit stronger hybridization with the orbitals of Mg and H, accompanied by more efficient electron transfer. This completely eliminates the band gap of Mg_4H_8 and significantly increases the electronic state density at the Fermi level, resulting in typical metallic properties. This also provides a structural basis for the improved electron transfer efficiency and the weakening of Mg–H bonds. These changes collectively lead to enhanced hydrogen evolution capability, reduced dehydrogenation enthalpy, and thus optimized hydrogen storage performance of MgH_2-based materials, consistent with the previously analyzed differential charge density results.

4 CONCLUSIONS

The synergistic catalytic effects of graphene combined with transition metal atoms (Sc, Fe, Cr, Ni, Cu) on MgH_2 dehydrogenation were systematically investigated using first-principles calculations. The results reveal that monolayer graphene modified with Ni, Cr, or Cu significantly decreases both the dehydrogenation enthalpy and activation energy of Mg_4H_8 clusters, confirming a pronounced synergistic catalytic interaction between these transition metals and graphene. Electronic structure analysis demonstrates that this catalysis strongly promotes charge redistribution between the monolayer graphene and the Mg_4H_8 cluster: adsorption-induced electron transfer from Mg to H notably elongates Mg–H bonds and weakens their bonding strength, thereby effectively facilitating hydrogen desorption. Among the three effective catalytic systems, Cu-modified monolayer graphene exhibits the most remarkable and superior performance – it achieves the greatest reduction in dehydrogenation enthalpy (1.2326 eV, 52.1% lower than pristine Mg_4H_8) while maintaining a balanced low activation energy (2.6199 eV), thereby realizing dual optimization of thermodynamic stability and kinetic reactivity. This superiority is further supported by unique electronic structure characteristics: Cu's d-orbital hybridization with Mg–H orbitals completely eliminates the 3.5 eV band gap of Mg_4H_8 and significantly enhances the density of electronic states at the Fermi level, promoting electron mobility and more effectively weakening Mg–H bonds compared to Ni- and Cr-modified systems.

Acknowledgements

This research was funded by the Future Industry Frontier Technology Project of Liaoning Province in 2025 (2025JH2/101330141), Key Research and Development Program of Liaoning Province in 2025 (2025JH2/101800416), and Fundamental Research Project of China National Nuclear Corporation (No. FK010261123429).

5 REFERENCES

[1] Z. Q. Zhang, J. W. Zheng, Prospects of China's hydrogen economy building and the countermeasures, Science and Society, (**2006**) 3, 21–25, doi:10.3969/j.issn.2095-1949.2006.03.004

[2] J. F. Zhao, Y. Q. Jiang, X. Zhan, X. N. Kong, Advances in research of impacts of aerosol pollution on crop in China, Advances in Meteorological Science and Technology, 8 (**2018**) 5, 6–10, doi:10.3969/j.issn.2095-1973.2018.05.001

[3] J. X. Zou, W. J. Ding, Review of research hotspots in magnesium-based hydrogen storage materials in 2023, Science & Technology Review, 42 (**2024**) 1, 204–216, doi:10.3981/j.issn.1000-7857.2024.01.013

[4] J. Q. Zhang, Current situation of hydrogen energy industry technology development in China, Boiler Manufacturing, (**2025**) 5, 56–58

[5] Y. Qin, X. L. Huang, L. Lin, Text analysis of China's hydrogen energy policies based on the LDA topic model, Resources and Industries, (**2025**), 1–23, doi:10.13776/j.cnki.resourcesindustries.20250901.002

[6] X. L. Ruan, X. D. Liao, S. Y. Liu, P. He, M. K. Li, Performance improvement and research progress of magnesium-based hydrogen storage materials, Dongfang Electric Review, 39 (**2025**) 4, 5–14, doi:10.13661/j.cnki.issn1001-9006.2025.04.003

[7] Q. Yuan, L. Y. Wang, Y. J. Lü, G. Q. Liu, Research progress of magnesium-based hydrogen storage materials, Chemical Industry and Engineering, 42 (**2025**) 3, 57–72, doi:10.13353/j.issn.1004.9533.20240525

[8] T. Sadhasivam, H. T. Kim, S. H. Jung, S. H. Roh, J. H. Park, H. Y. Jung, Dimensional effects of nanostructured Mg/MgH_2 for hydrogen storage applications: a review, Renewable and Sustainable Energy Reviews, 72 (**2017**), 523-534, doi:10.1016/j.rser.2017.01.107

[9] K. F. Aguey-Zinsou, J. Ares-Fernandez, Hydrogen in magnesium: new perspectives to ward functional stores, Energy & Environmental Science, 3 (**2010**) 5, 526–543, doi:10.1039/B921645F

[10] M. J. Yang, X. Q. Zhu, L. L. Zhou, Q. Deng, C. Wei, Hydrogen storage performance of graphene and its application in magnesium-based hydrogen storage materials, New Chemical Materials, 49 (**2021**) 1, 23–27, doi:10.19817/j.cnki.issn1006-3536.2021.01.006

[11] G. Liu, Y. J. Wang, L. F. Jiao, H. T. Yuan, Understanding the role of few-layer graphene nanosheets in enhancing the hydrogen sorption kinetics of magnesium hydride, ACS Applied Materials & Interfaces, 6 (**2014**) 14, 11038–11046, doi:10.1021/am502755s

[12] M. J. Liu, S. C. Zhao, X. Z. Xiao, M. Chen, C. Sun, Z. Yao, Novel 1D carbon nanotubes uniformly wrapped nanoscale MgH_2 for efficient hydrogen storage cycling performances with extreme high gravimetric and volumetric capacities, Nano Energy, 61 (**2019**), 540–549, doi:10.1016/j.nanoen.2019.04.094

[13] M. M. Hu, X. B. Xie, M. Chen, C. Zhu, T. Liu, TiCX-decorated Mg nanoparticles confined in carbon shell: preparation and catalytic mechanism for hydrogen storage, Journal of Alloys and Compounds, 817 (**2020**), 152813, doi:10.1016/j.jallcom.2019.152813

[14] G. S. Zhu, X. M. Du, Effects of Sc/Cu and Sc/Zn co-doping on the hydrogenation/dehydrogenation properties of Mg-based hydrogen storage materials: A theoretical study, International Journal of Hydrogen Energy, 60 (**2024**), 515–523, doi:10.1016/j.ijhydene.2024.02.134

[15] G. S. Zhu, X. M. Du, F. Li, Effect of Sc on the hydrogen-storage performance of Mg_2Ni: A first-principles study, Materials and Technology, 58 (**2024**) 1, 95–101, doi:10.17222/mit.2023.980

[16] X. M. Du, G. S. Zhu, D. D. Sun, First-principles investigation of the effects of Y/Cu and Y/Zn co-doping on the hydrogenation/dehydrogenation properties of Mg_2Ni alloy, Journal of Physics and Chemistry of Solids, 202 (**2025**), 112661, doi:10.1016/j.jpcs.2025.112661

[17] M. E. Khatabi, M. Bhihi, S. Naji, H. Labrim, A. Benyoussef, A. E. Kenz, M. Loulidi, Study of doping effects with 3d and 4d-transition metals on the hydrogen storage properties of MgH_2, International

Journal of Hydrogen Energy, 41 (**2016**) 8, 4712–4718, doi:10.1016/j.ijhydene.2016.01.001

[18] G. L. Xia, Y. B. Tan, X. W. Chen, D. L. Sun, Z. P. Guo, H. K. Liu, L. Z. Ouyang, M. Zhu, X. B. Yu, Monodisperse magnesium hydride nanoparticles uniformly self-assembled on graphene, Advanced Materials, 27 (**2015**) 39, 5981–5988, doi:10.1002/adma.201502005

[19] J. Cui, H. Wang, J. W. Liu, L. Z. Ouyang, Q. G. Zhang, D. L. Sun, X. D. Yao, M. Zhu, Remarkable enhancement in dehydrogenation of MgH_2 by a nano-coating of multi-valence Ti-based catalysts, Journal of Materials Chemistry A, 1 (**2013**) 18, 5603, doi:10.1039/c3ta01332d

[20] J. Zhang, H. Ou, G. Wu, L. B. Song, X. F. Yu, D. W. Zhou, Remarkably enhanced dehydrogenation properties and mechanisms of MgH_2 by sequential-doping of nickel and graphene, International Journal of Hydrogen Energy, 41 (**2016**) 39, 17433–17441, doi:10.1016/j.ijhydene.2016.07.204

[21] P. Giannozzi, S. Baroni, N. Bonini, M. Calandra, R. Car, C. Cavazzoni, D. Ceresoli, G. L. Chiarotti, M. Cococcioni, I. Dabo, A. D. Corso, S. De Gironcoli, S. Fabris, G. Fratesi, R. Gebauer, U. Gerstmann, C. Gougoussis, A. Kokalj, M. Lazzeri, L. Martin-Samos, N. Marzari, F. Mauri, R. Mazzarello, S. Paolini, A. Pasquarello, L. Paulatto, C. Sbraccia, S. Scandolo, G. Sclauzero, A. P. Seitsonen, A. Smogunov, P. Umari, R. M. Wentzcovitch, Quantum espresso: a modular and open-source software project for quantum simulations of materials, Journal of Physics: Condensed Matter, 21 (**2009**) 39, 395502, doi:10.1088/0953-8984/21/39/395502

[22] J. P. Perdew, J. A. Chevary, S. H. Vosko, K. A. Jackson, M. R. Pederson, D. J. Singh, C. Fiolhais, Atoms, molecules, solids, and surfaces: applications of the generalized gradient approximation for exchange and correlation, Physical Review B, 46 (**1992**) 11, 6671–6687, doi:10.1103/physrevb.46.6671

[23] M. A. Nosir, L. Martin-Gondre, G. A. Bocan, R. D. Muiño, Adsorption dynamics of molecular nitrogen at an Fe (111) surface, Physical Chemistry Chemical Physics, 19 (**2017**) 10, 7370–7379, doi:10.1039/C6CP07174K

[24] A. Majid, S. Tasawar, H. Raza, K. Alam, M. Alkhedher, S. Haider, N. Ahmed, Uncovering the potential of two-dimensional $SrRuO_3$ as anode material in Li, Na, Mg, Ca, K, and Zn ion batteries: first-principles investigations of structural, electronic and electrochemical properties, Journal of Energy Storage, 105 (**2024**), 114634, doi:10.1016/j.est.2024.114634

[25] Y. Jiang, J. B. Adams, First principle calculations of benzotriazole adsorption onto clean Cu(1 1 1), Surface Science, 529 (**2003**) 3, 428–442, doi:10.1016/S0039-6028(03)00277-2

[26] A. Züttel, Materials for hydrogen storage, Materials Today, 6 (**2003**) 9, 24–33, doi:10.1016/S1369-7021(03)00922-2

[27] N. Hanada, T. Ichikawa, H. Fujii, Catalytic effect of nanoparticle 3d-transition metals on hydrogen storage properties in magnesium hydrogen MgH_2 prepared by mechanical milling, The Journal of Physical Chemistry B, 109 (**2005**) 15, 7188–7194, doi:10.1021/jp044576c

[28] Q. Q. Huan, Y. F. Zhu, L. J. Wei, L. Q. Li, Hydrogen storage properties of Mg–Ni/graphene composites, Rare Metal Materials and Engineering, 43 (**2014**) 2, 356–360, doi:10.12442/j.issn.1002-185X.2014.43.2.356360

[29] J. Zhang, X. F. Yu, C. Mao, C. G. Long, J. Chen, D. W. Zhou, Influences and mechanisms of graphene-doping on dehydrogenation properties of MgH_2: Experimental and first-principles studies, Energy, 89 (**2015**), 957–964, doi:10.1016/j.energy.2015.06.037

[30] G. Henkelman, B. P. Uberuaga, H. Jónsson, A climbing image nudged elastic band method for finding saddle points and minimum energy paths, The Journal of Chemical Physics, 113 (**2000**) 22, 9901–9904, doi:10.1063/1.1329672

[31] S. Dong, E. F. Lv, J. H. Wang, C. Q. Li, K. Ma, Z. Y. Gao, W. J. Yang, Z. Ding, C. C. Wu, I. D. Gates, Construction of transition metal-decorated boron doped twin-graphene for hydrogen storage: a theoretical prediction, Fuel, 304 (**2021**), 121351, doi:10.1016/j.fuel.2021.121351

[32] Y. He, L. Ding, X. Wu, Q. L. Li, Z. Q. Li, W. P. Zhang, S. W. Jin, Hydrogen release mechanisms of MgH_2 over NiN_4-embedded graphene nanosheet: First-principles calculations, International Journal of Hydrogen Energy, 47 (**2022**) 93, 39549–39562, doi:10.1016/j.ijhydene.2022.09.102

[33] H. P. Zhang, X. G. Luo, X. Y. Lin, P. P. Tang, X. Lu, L. M. Fang, Y. H. Tang, Modulating the interactions between MgH_2 and graphene using different dopants, Chemical Physics Letters, 623 (**2015**), 82–88, doi:10.1016/j.cplett.2015.01.052